BUD23 is associated with malignancy and correlates with immune infiltration in NSCLC

YONGHUANG TAN[1*], JUN MA[1*], JIANGLI ZHOU[2] and JIANJUN LU[1]

[1]Department of Thoracic Surgery, The First Affiliated Hospital, Sun Yat-sen University, Guangzhou, Guangdong 510080, P.R. China; [2]Guangdong Key Laboratory of Chiral Molecule and Drug Discovery, and Guangdong Provincial Key Laboratory of New Drug Design and Evaluation, School of Pharmaceutical Sciences, Sun Yat-sen University, Guangzhou, Guangdong 510006, P.R. China

Received October 9, 2025; Accepted March 10, 2026

DOI: 10.3892/ol.2026.15608

Abstract. Lung cancer remains the primary cause of cancer-related mortality worldwide. BUD23, also known as Williams-Beuren syndrome critical region 22, is an rRNA methyltransferase involved in ribosome maturation and RNA methylation. It has been reported to promote tumor progression in several malignancies. Although BUD23 has been implicated in drug resistance in lung cancer cells, its role in non-small cell lung cancer (NSCLC) remains incompletely understood. In the present study, transcriptomic and proteomic datasets were analyzed to evaluate the expression of BUD23 in NSCLC and normal tissues, and Kaplan-Meier survival analysis was performed to assess its prognostic significance. Immune infiltration algorithms were used to examine the correlation between BUD23 expression and tumor immune cell infiltration in NSCLC. Gene set enrichment analysis (GSEA), Kyoto Encyclopedia of Genes and Genomes (KEGG) pathway analysis and single-cell enrichment analysis were conducted to explore the biological pathways associated with BUD23 expression. *In vitro*, the effect of BUD23 knockdown on the viability, motility and apoptosis of NSCLC cell lines was evaluated by Cell Counting Kit-8, wound healing and Annexin V/PI flow cytometry assays, respectively, and the mRNA expression levels of potential downstream genes were quantified by reverse transcription-quantitative PCR. BUD23 was found to be significantly upregulated in NSCLC and associated with poor patient survival. Immunogenomic analyses indicated that high BUD23 levels are correlated with reduced immune cell infiltration. GSEA, KEGG and single-cell pathway enrichment analyses consistently implicated BUD23 in 'DNA repair' and 'cell cycle' pathways. *In vitro*, BUD23 knockdown suppressed the proliferation and migration of NSCLC cells, and reduced RNA polymerase II subunit J expression. Collectively, these findings suggest that BUD23 may contribute to the development and progression of NSCLC, and provide a strong basis for future mechanistic and clinical investigations.

Correspondence to: Dr Jianjun Lu, Department of Thoracic Surgery, The First Affiliated Hospital, Sun Yat-sen University, 58 Zhongshan Er Road, Guangzhou, Guangdong 510080, P.R. China
E-mail: lujj@mail.sysu.edu.cn

*Contributed equally

Key words: NSCLC, BUD23, prognosis, immune infiltration, malignancy, cancer

Introduction

Lung cancer is the leading cause of cancer-related mortality worldwide, with an estimated 2.5 million new cases and 1.8 million deaths annually (1). Non-small cell lung cancer (NSCLC) is the most prevalent histological subtype, accounting for ~85% of all lung cancer cases. Among NSCLC subtypes, lung adenocarcinoma (LUAD) and lung squamous cell carcinoma (LUSC/LSCC) are the most prevalent (2). Despite advancements in lung cancer treatment strategies, the prognosis for patients with inoperable NSCLC remains poor, with a 5-year survival rate ranging from 13 to 60% (3-5). Consequently, elucidation of the molecular mechanisms underlying the development and progression NSCLC is critical for improving the outcomes of patients with this disease.

BUD23, also known as Williams-Beuren syndrome critical region 22, is a member of the rRNA methyltransferase family that functions as a ribosome maturation factor and was initially identified in patients with Williams-Beuren syndrome (6). Current evidence indicates that that BUD23 acts as a methyltransferase and plays a crucial role in RNA methylation (7,8). In addition, it has a confirmed involvement in ribosome biogenesis (7,9).

Several studies have suggested that BUD23 contributes to tumorigenesis. For example, high BUD23 expression has been associated with poor prognosis in patients with glioblastoma (10). In addition, BUD23 contributes to the survival of multiple myeloma cells, and its knockdown significantly impairs cell proliferation and invasive capacity, and its knockdown significantly impairs cell proliferation and invasive capacity (11). In breast cancer, BUD23 promotes metastasis by inhibiting Zac1/p53-dependent apoptosis (12). Conversely, BUD23 and tRNA methyltransferase activator subunit 11-2 together inhibit pancreatic cancer cell proliferation, invasion and tumorigenesis through the transcriptional regulation of interferon-stimulated gene 15 (13). In lung cancer cells, BUD23

has been implicated in drug resistance, as the knockdown of BUD23 reduces the sensitivity of H460 NSCLC cells to the active camptothecin metabolite 7-ethyl-10-hydroxycamptothecin and 5-fluorouracil (14). However, despite its involvement in multiple cancer types, the precise role of BUD23 in NSCLC remains to be elucidated and warrants further investigation.

In the present study, transcriptomics and proteomics profiling was performed to evaluate the expression of BUD23 in NSCLC, and its association with patient outcomes was assessed. Integrative immunogenomic analysis was conducted to evaluate the association of BUD23 levels with tumor immune infiltration. Gene Set Enrichment Analysis (GSEA), Kyoto Encyclopedia of Genes and Genomes (KEGG) and single-cell pathway enrichment analyses were also performed to identify the pathways associated with BUD23. In addition, the effect of BUD23 knockdown on the proliferation and migration of NSCLC cells was evaluated *in vitro*, and its potential downstream genes were identified and verified. The findings are intended to provide a basis for future research into the role of BUD23 in the development and progression of NSCLC.

Materials and methods

Expression analysis of BUD23. Differences in the expression of BUD23 between tumor and normal tissues were analyzed using standardized data from The Cancer Genome Atlas (TCGA), including TCGA-LUAD and TCGA-LUSC cohorts. The TCGA data downloaded from GEPIA2 (http://gepia2.cancer-pku.cn/#index) completed standardization. Additionally, two proteomic datasets derived from lung cancer samples were retrieved from the National Cancer Institute's Clinical Proteomic Tumor Analysis Consortium (CPTAC: https://pdc.cancer.gov/pdc), namely the CPTAC LSCC Discovery Study and CPTAC LUAD Discovery Study (15,16).

Gene expression omnibus (GEO) dataset processing. The datasets GSE30219 (17), GSE19188 (18), GSE40791 (19), GSE32665 (20), GSE40419 (21), GSE75037 (22), GSE7670 (23), GSE27262 (24), GSE63459 (25), GSE87340 (26), GSE31547 (27) and GSE31210 (28), including their matrix and platform information, were obtained from the GEO database (http://www.ncbi.nlm.nih.gov/geo). We used the gene identifiers provided by the probe platform, as well as the expression values in the data matrix. All expression matrices have undergone normalization by GEO submitters.

Survival analysis. The Kaplan-Meier plotter tool (http://kmplot.com/analysis/) was used to evaluate the association of BUD23 expression with survival (29). BUD23 (Affymetrix ID 207628_s_at) was also subjected to univariate and multivariate Cox regression analyses within the lung cancer module. The patient population was segmented using the 'Auto select the best cutoff' feature. Kaplan-Meier survival curves were generated for overall survival (OS), post-progression survival (PPS) and first progression survival (FPS). $P<0.05$ was considered to indicate statistical significance.

Immune infiltration analysis in NSCLC from Sangerbox 2.0 (http://sangerbox.com/). To assess the extent of immune infiltration associated with UD23 expression in NSCLC, several online analysis platforms utilizing TCGA-LUAD and -LUSC datasets were employed. Specifically, correlations between BUD23 expression and immune cell infiltration levels were analyzed using TIMER, EPIC, MCPcounter and QUANTISEQ algorithms (30-33). The correlations of BUD23 expression with stromal, immune and ESTIMATE scores were further investigated using the ESTIMATE algorithm (34). Additionally, the Immunophenoscore (IPS), calculated using the IPS algorithm, was used to evaluate the correlation between BUD23 expression and various components associated with tumor immunogenicity in NSCLC (35).

Correlation analysis using UALCAN. UALCAN (https://ualcan.path.uab.edu/) was used to identify the genes that significantly correlated with BUD23 in the 'TCGA' module (36). After inputting 'BUD23' as the Gene Symbol and selecting the 'Correlation analysis' module, the analysis results were downloaded for both LUAD and LUSC. Genes with extremely low expression (median transcripts per million <0.5) were excluded from the list, and only those with $R^2 \geq 0.3$ and $P<0.05$ were included in the final sets. This yielded 134 significantly correlated genes in LUAD and 165 in LUSC.

Correlation analysis using Metascape. The KEGG enrichment analysis was performed utilizing Metascape (https://metascape.org/gp/index.html#/main/step1). All enrichment parameters were set as the default values (Min Overlap: 3; P-value Cutoff: 0.01; Min Enrichment: 1.5), and the KEGG Pathway database was selected as the enrichment dataset for subsequent analysis.

GSEA pathway enrichment analysis. TCGA-LUAD and -LUSC data were analyzed by GSEA. The patients were divided into BUD23 high and low groups according to the median expression level of BUD23 within each cohort. The Hallmark gene sets were used for GSEA analysis. GSEA software (v3.0) was obtained from the official website (DOI:10.1073/pnas.0506580102; http://software.broadinstitute.org/gsea/index.jsp). Samples were stratified into high and low BUD23 expression groups by the 50% cutoff. The h.all.v7.4.symbols.gmt gene set was downloaded from MSigDB (DOI:10.1093/bioinformatics/btr260; http://www.gsea-msigdb.org/gsea/downloads.jsp). Parameters were set as: Minimum gene set size=5, maximum=5,000 and 1,000 permutations. $P<0.05$ and FDR <0.25 were considered statistically significant. $P<0.05$ was considered to be statistically significant.

Single-cell analysis of BUD23 in NSCLC. The CancerSEA online database (http://biocc.hrbmu.edu.cn/CancerSEA/home.jsp) was used to examine the association of BUD23 with 14 different functional states of NSCLC at single-cell resolution in the E-MTAB-6149 dataset (37). These functional states encompass angiogenesis, apoptosis, invasion, epithelial-mesenchymal transition, differentiation, proliferation, DNA damage, metastasis, hypoxia, inflammation, cell cycle progression, DNA repair, stemness and quiescence.

Cell culture and cell transfection. The HBE [full name: HBE4-E6/E7 (Human Bronchial Epithelial Cells; cat. no. CRL-2078)] cell line, A549 lung adenocarcinoma cell

line (cat. no. CCL-185), H1299 lung large cell carcinoma cell line (cat. no. CRL-5803), H460 lung large cell carcinoma cell line (cat. no. HTB-177) and Jurkat T cells (cat. no. TIB-152; a childhood T acute lymphoblastic leukemia T-cell line), were purchased from the American Type Culture Collection. Cells were cultured and maintained in RPMI-1640 (cat. no. PM150110; Procell Life Science & Technology Co., Ltd.) supplemented with 10% fetal bovine serum (FBS; cat. no. 164210-50; Procell Life Science & Technology Co., Ltd.), 100 U/ml penicillin and 100 μg/ml streptomycin, and were incubated in a humidified chamber at 37˚C with 95% air and 5% CO_2.

BUD23-small interfering RNAs (siRNAs) and negative control siRNA were obtained from Guangzhou RiboBio. The BUD23 siRNAs were as follows: Si1 sense, 5'GTGGTA GACTACCCTAACA3' and antisense: 5'CAUCACCUG AGUCGAGUCUU3'; Si2 sense, 5'CAGTGGCTCTGTAAT GCTA3' and antisense, 5'GUCACCACAUCAUCAGCAU3'. The specific sequence of the negative control siRNA (cat. no. siN0000002-1-5) was not disclosed by the supplier. The A549 and H1299 cells were transfected at 50-60% confluency. The transfection was performed using Lipo8000 transfection reagent (cat. no. C0533; Beyotime Institute of Biotechnology). The nucleic acid mass used was 2 μg per well. Transfection was carried out at 37˚C for 6 h and the subsequent experiments were performed 24 h after transfection.

Transwell co-culture assay. Transwell co-culture was conducted with 0.4 μm pore Transwell inserts (cat. no. 3413; Corning, Inc.); this pore size enables soluble factor exchange without direct cell contact. A549/H1299 cells underwent BUD23 knockdown for 24 h and were then seeded into the lower chamber at $5x10^4$ cells/well with DMEM (10% FBS). Jurkat T cells (cultured in RPMI 1640 with 10% FBS) were added to the upper inserts at $1x10^5$ cells/insert, followed by 48 h co-culture at 37˚C with 5% CO_2. Control groups consisted of BUD23-knockdown A549/H1299 cells cultured alone under the same conditions. After co-culture, lower-chamber A549/H1299 cells were washed with cold PBS and harvested for downstream assays.

Wound-healing assays. Following the knockdown of BUD23, A549 and H1299 cells were seeded on 6-well plates and allowed to reach 80-90% confluence. Then, the cell monolayers were scratched with a 200-μl pipette tip, and culture was maintained in RPMI-1640 supplemented with 1% FBS. The migration distance of the cells was measured at 0, 24 and 48 h. Wound images were captured using an inverted phase-contrast microscope. The wound closure rate was quantified by measuring the wound width at 0, 24 and 48 h with ImageJ software (version 1.54r; National Institutes of Health), and the relative migration rate was calculated accordingly.

Cell counting kit-8 (CCK-8) assay. Cell viability was quantified using a CCK-8 assay (Dojindo Laboratories, Inc.). Following the siRNA-mediated knockdown of BUD23, A549 cells and H1299 were seeded in 96-well plates (3,000 or 2,000 cells/well, respectively; 5 replicates per group) and cultured for 24 or 48 h (the time when cells were transferred into 48-well plates and allowed to adhere was set as 0 h). Subsequently, 10 μl CCK-8 reagent was added to each well and the plate was incubated for 1 h at 37˚C in 5% CO_2. Absorbance at 450 nm was measured using a microplate reader (BioTek Synergy H1; Agilent Technologies, Inc.).

Apoptosis assay. Following BUD23 knockdown, A549 and H1299 cells were seeded in 6-well plates at 70% confluence for 8 h, and then processed using an Annexin V-FITC Apoptosis Detection Kit (Cat. No. AD10, lot SH680; Dojindo Laboratories, Inc.). Flow cytometric analysis was performed using a BD FACSCalibur flow cytometer (BD Biosciences). Data were analyzed using FlowJo software (version 10.8.1; BD Life Sciences). The percentages of early and late apoptotic cells were calculated for each sample. The cells in quadrants Q2 (late apoptosis) and Q3 (early apoptosis) were considered to be apoptotic and were subjected to analysis.

Cell cycle analysis. Cell cycle distribution in H1299 and A549 cells was detected using the Cell Cycle and Apoptosis Analysis Kit (cat. no. C1052, Beyotime Institute of Biotechnology) in strict accordance with the manufacturer's instructions. Cells were harvested, fixed with pre-chilled 70% ethanol overnight at 4˚C, washed with cold PBS and stained with PI/RNase A staining buffer at 37˚C for 30 min in the dark. Flow cytometry was conducted for detection and data were analyzed using FlowJo software (version 10.8.1) to calculate the percentage of cells in G0/G1, S and G2/M phases.

Reverse transcription-quantitative PCR (RT-qPCR). RNA was extracted from the cells using TRIzol® (Invitrogen; Thermo Fisher Scientific, Inc.). RT was performed using the PrimeScript™ RT Reagent Kit with gDNA Eraser (Perfect Real Time; cat. no. RR047A; TaKaRa Bio Inc.) containing reverse transcriptase, RT buffer, dNTP mix, oligo(dT) primers, random primers and gDNA Eraser. The cDNA synthesis was performed strictly according to the manufacturer's protocol and cDNA was stored at -20˚C for qPCR analysis. The qPCR analyses were performed using SYBR Premix Ex Taq (Takara Bio, Inc.) according to the manufacturer's instructions [the thermal cycling protocol was as follows: 42˚C for 2 min (gDNA removal), 37˚C for 15 min (cDNA synthesis) and 85˚C for 5 sec (enzyme inactivation). cDNA was stored at -20˚C for qPCR analysis) and quantified using a CFX96 Real-Time PCR System (Bio-Rad Laboratories, Inc.). Relative fold changes in expression were calculated using the $2^{-\Delta\Delta Cq}$ method (38). The primer pairs used for qPCR are listed in Table SI.

Statistical analysis. All statistical analyses were performed using SPSS software (version 29.0; IBM Corp.). Student's t-tests were used to analyze the differences between two groups, with an unpaired t-test used for independent samples and paired t-test for paired samples. One-way analysis of variance followed by Tukey's post-hoc test was used for the comparison of three or more groups. Pearson's correlation analysis was performed to assess correlations among variables. Data are presented as mean ± standard deviation from three independent replicates. $P<0.05$ was considered to indicate a statistically significant result.

Results

BUD23 is highly expressed in NSCLC based on TCGA, GTEx and CPTAC data. The mRNA expression profile of BUD23 in various cancers was examined using data on human cancer tissue from TCGA database. This analysis revealed that BUD23 mRNA was significantly upregulated in LUAD and LUSC tissues relative to that in normal lung tissues (Fig. 1A). Given the limited number of normal tissue samples in TCGA, the TCGA data were supplemented with samples from the GTEx database through the GEPIA2 platform. This allowed a more comprehensive comparison of BUD23 expression between normal lung and lung tumor tissues. The results indicated that BUD23 expression was significantly upregulated in LUAD and LUSC (fold change >1.5, P<0.01; Fig. 1B and C). In addition, BUD23 protein expression levels in LUAD and LUSC tissues were compared with those in normal tissues using CPTAC proteomics data. Consistent with the mRNA findings, BUD23 protein levels were significantly elevated in tumor tissues compared with normal tissues (Fig. 1D and E). Collectively, these analyses demonstrate that BUD23 is highly expressed in NSCLC.

BUD23 is highly expressed in NSCLC based on GEO datasets. To examine the differential expression of BUD23 in NSCLC, multiple publicly available gene expression datasets from the GEO database were analyzed. BUD23 expression was confirmed to be significantly upregulated in tumor tissues compared with normal tissues in multiple NSCLC cohorts, namely those in the GSE19188, GSE30219, GSE40791, GSE32665, GSE40419, GSE75037, GSE7670, GSE27262, GSE63459 and GSE87340 datasets. This stable upregulation was observed regardless of whether the samples were unmatched: Tumor and adjacent normal tissues were from different patients (Fig. 2A-C) or matched: Tumor and adjacent normal tissues were from the same patient (Fig. 2D-J), indicating a consistent and significant upregulation of BUD23 expression in NSCLC. These analyses suggest that BUD23 may play a role in the development or progression of NSCLC.

Elevated BUD23 levels are associated with poor clinical outcomes in patients with NSCLC. The association between BUD23 expression and patient prognosis was analyzed using the Kaplan-Meier plotter, which encompasses 17 NSCLC datasets. The analysis verified that elevated BUD23 expression was significantly associated with shorter OS [high vs. low; hazard ratio (HR), 1.43; 95% CI, 1.25-1.64; P<0.05; n=2,166; Fig. 3A], FPS (high vs. low; HR, 1.61, 95% CI, 1.3-2.0; P<0.05; n=1,252; Fig. 3B) and PPS (high vs. low; HR, 1.58; 95%CI, 1.27-1.97; P<0.05; n=477; Fig. 3C). Furthermore, the association between BUD23 expression and OS was explored in patients with NSCLC stratified by N stage. The results revealed that BUD23 expression was not associated with OS in patients with N0 stage NSCLC (Fig. 3D). However, elevated BUD23 expression was significantly associated with poor OS in patients with stages N1 (high vs. low; HR, 1.52; 95% CI, 1.05-2.19; P<0.05; Fig. 3E) and N2 (high vs. low; HR, 1.7; 95%CI, 1.05-2.74; P<0.05; Fig. 3F). Multivariate regression analysis also indicated that BUD23 expression is associated with a poor prognosis for OS (high vs. low; HR,1.61; 95% CI, 1.22-2.13; P<0.05) and PPS (high vs. low; HR, 1.92; 95% CI, 1.36-2.72; P<0.05) (Table I). The association between BUD23 expression and clinical stage was also investigated. The analysis of GSE40419, GSE31547 and GSE31210 datasets revealed a significant elevation in BUD23 expression as the clinical stage advanced (Fig. 3G-I). In conclusion, elevated BUD23 levels are associated with worse clinical outcomes in patients with NSCLC.

Immune characteristics of BUD23 in NSCLC. Immune infiltration serves as an independent prognostic indicator in tumors (39). Consequently, the correlations between BUD23 expression and immune cell infiltration levels in TCGA-LUAD and -LUSC cohorts were examined using the TIMER tool. The results indicated that BUD23 expression is significantly negatively correlated with B cell, $CD8^+$ T cell and macrophage counts in LUAD, while in LUSC, BUD23 expression is significantly negatively correlated with B cell, $CD8^+$ T cell, neutrophil, macrophage and dendritic cell counts (Fig. 4A). In addition, immune characterization analyses performed using EPIC (Fig. 4B), MCPcounter (Fig. 4C) and QUANTISEQ (Fig. 4D) further confirmed that BUD23 expression is negatively correlated with the infiltration of B cells (all three methods; Fig. 4B-D), CD8+ T cell infiltration (MCPcounter and QUANTISEQ; Fig. 4C and D) and macrophage infiltration (QUANTISEQ; Fig. 4D). The IPS is a metric used to evaluate tumor immunogenicity, with higher IPS values indicating greater immunogenic potential. Assessment of the correlation between BUD23 expression and IPS revealed that BUD23 is negatively correlated with IPS in LUSC (Fig. 4E), suggesting that LUSC tumors with high BUD23 expression are less immunogenic. Furthermore, the correlations of BUD23 expression with stromal and immune cell levels were evaluated using the ESTIMATE algorithm. High BUD23 expression was found to be negatively correlated with stromal, immune and ESTIMATE scores in NSCLC (Fig. 4F-H), indicating that patients with elevated BUD23 expression have higher tumor purity. Collectively, these findings demonstrate that BUD23 is negatively associated with immune cell infiltration.

BUD23 may be involved in DNA repair and cell cycle pathways and associated with NSCLC malignancy. To elucidate the potential downstream effects and molecular mechanisms of BUD23 in NSCLC, GSEA was performed to compare patients with high and low BUD23 expression levels in TCGA-LUAD and -LUSC cohorts. The analysis demonstrated that the Hallmark 'DNA repair' gene set was significantly enriched in patients with elevated BUD23 expression in both cohorts (Fig. 5A and B). Correlation analyses were performed in TCGA-LUAD and -LUSC cohorts to screen out the genes that exhibit a positive correlation with BUD23 ($R^2 \geq 0.3$, P<0.05), and KEGG enrichment analyses were conducted to identify the pathways associated with BUD23-related genes. The results indicate that BUD23-related genes are enriched in the 'cell cycle' signaling pathway in both LUAD and LUSC (Fig. 5C and D). Moreover, to elucidate the correlation of BUD23 expression with cancer functional states in NSCLC at single-cell resolution, an analysis was conducted via CancerSEA based on the E-MTAB-6149 dataset. The

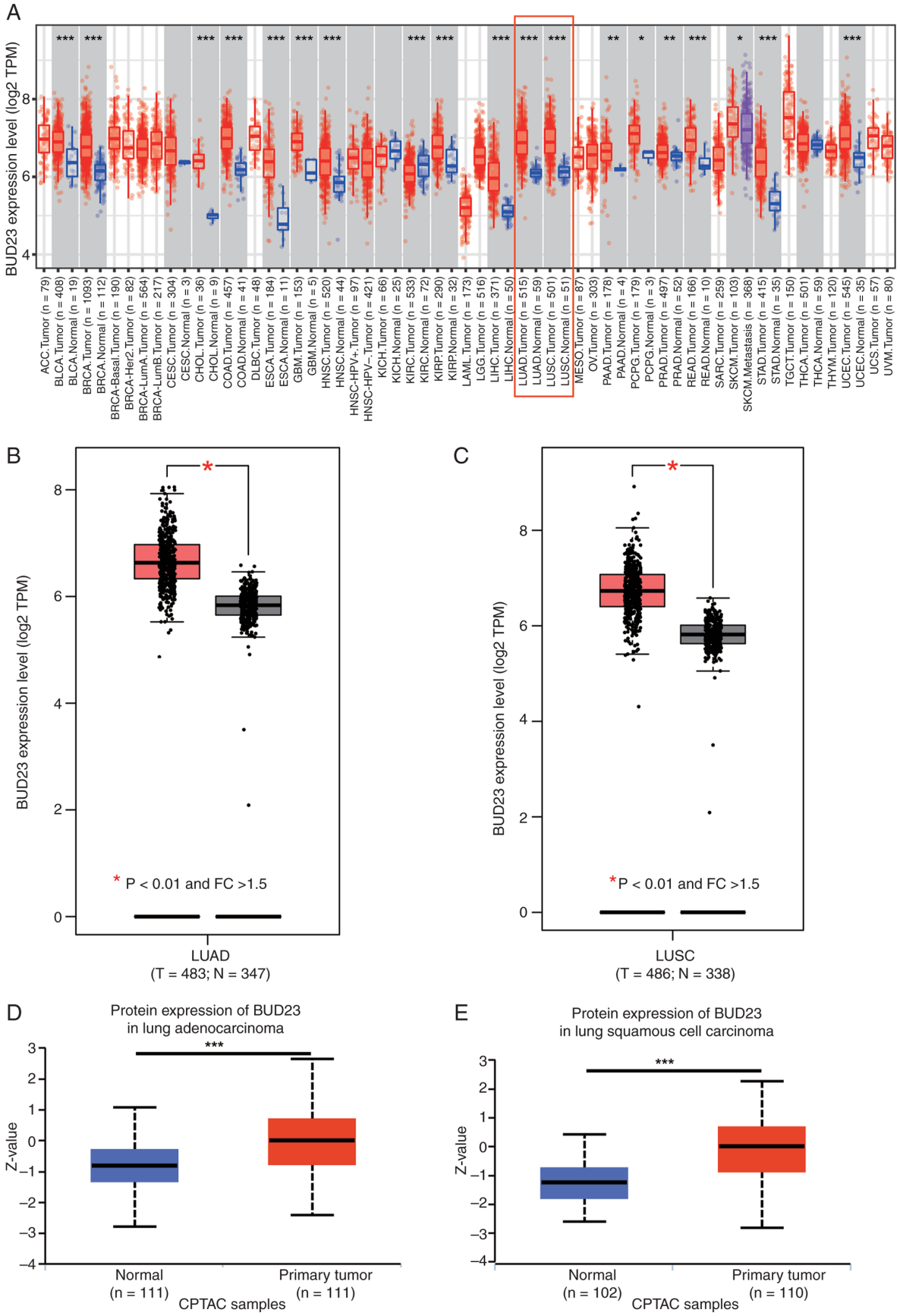

Figure 1. BUD23 expression is upregulated in NSCLC based on TCGA, GTEx and CPTAC data. (A) Pan-cancer analysis of BUD23 expression in tumor and normal tissues based on TCGA data. Expression analysis of BUD23 in (B) LUAD and (C) LUSC between cancer and normal tissues based on integrated TCGA and GTEx datasets. Protein expression analysis of BUD23 in (D) lung adenocarcinoma or (E) lung squamous cell carcinoma compared with that in normal tissues based on CPTAC data. *P<0.05, **P<0.01 and ***P<0.001 as indicated. NSCLC, non-small cell lung cancer; TCGA, The Cancer Genome Atlas; GTEx, Genotype-Tissue Expression; CPTAC, Clinical Proteomic Tumor Analysis Consortium; LUAD, lung adenocarcinoma; LUSC, lung squamous cell carcinoma; TPM, transcripts per million; FC, fold change; T, tumor; N, normal.

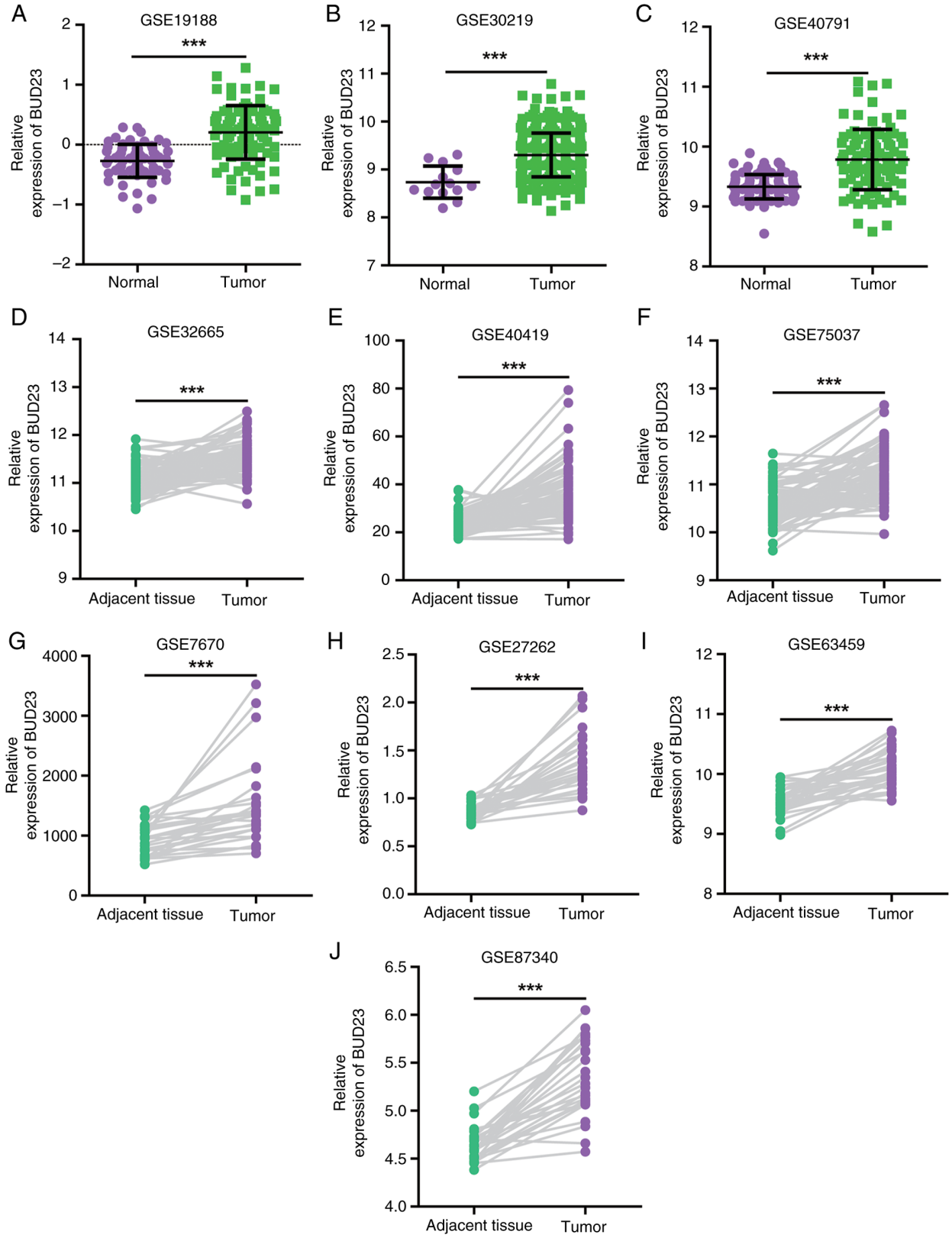

Figure 2. BUD23 expression is upregulated in NSCLC based on GEO dataset analyses. mRNA expression levels of BUD23 in normal lung and primary NSCLC tissue based on GEO datasets (A) GSE19188, (B) GSE30219 and (C) GSE40791. Expression levels of BUD23 in lung cancer and matched adjacent normal tissues from GEO datasets (D), GSE32665, (E) GSE40419, (F) GSE75037, (G) GSE7670, (H) GSE27262, (I) GSE63459 and (J) GSE87340. ***P<0.001 as indicated. NSCLC, non-small cell lung cancer; GEO, Gene Expression Omnibus.

expression of BUD23 was found to be positively correlated with cell cycle activity scores (R^2=0.2138, P<0.05) and DNA repair activity scores (R^2=0.1263, P<0.05; Fig. 5E and F, respectively). These findings further suggest that BUD23 is involved in 'DNA repair' and 'cell cycle' pathways and is associated with NSCLC malignancy.

Table I. Multivariate analysis of BUD23 expression in patients with non-small cell lung cancer.

	Overall survival		First progression survival		Post-progression survival	
Factor	P-value	Hazard ratio	P-value	Hazard ratio	P-value	Hazard ratio
Histology	0.5294	0.91 (0.67-1.22)	-	-	-	-
Grade	0.9248	1.01 (0.82-1.24)	0.4984	0.92 (0.73-1.17)	0.8174	0.97 (0.75-1.26)
AJCC T stage	0.0004	1.42 (1.17-1.72)	0.0012	1.51 (1.18-1.93)	0.0032	1.52 (1.15-2.01)
AJCC N stage	<0.0001	1.85 (1.57-2.19)	<0.0001	1.57 (1.27-1.93)	0.0017	1.43 (1.14-1.78)
Sex (male vs. female)	0.1264	1.23 (0.94-1.60)	0.5043	1.11 (0.81-1.53)	0.8213	1.04 (0.74-1.47)
Smoking history	0.2346	0.75 (0.47-1.20)	0.3323	0.79 (0.49-1.27)	0.8330	1.06 (0.62-1.81)
BUD23	0.0007	1.61 (1.22-2.13)	0.0989	1.32 (0.95-1.84)	0.0002	1.92 (1.36-2.72)

Analysis was performed using the Kaplan-Meier plotter database and tool. AJCC, American Joint Committee on Cancer.

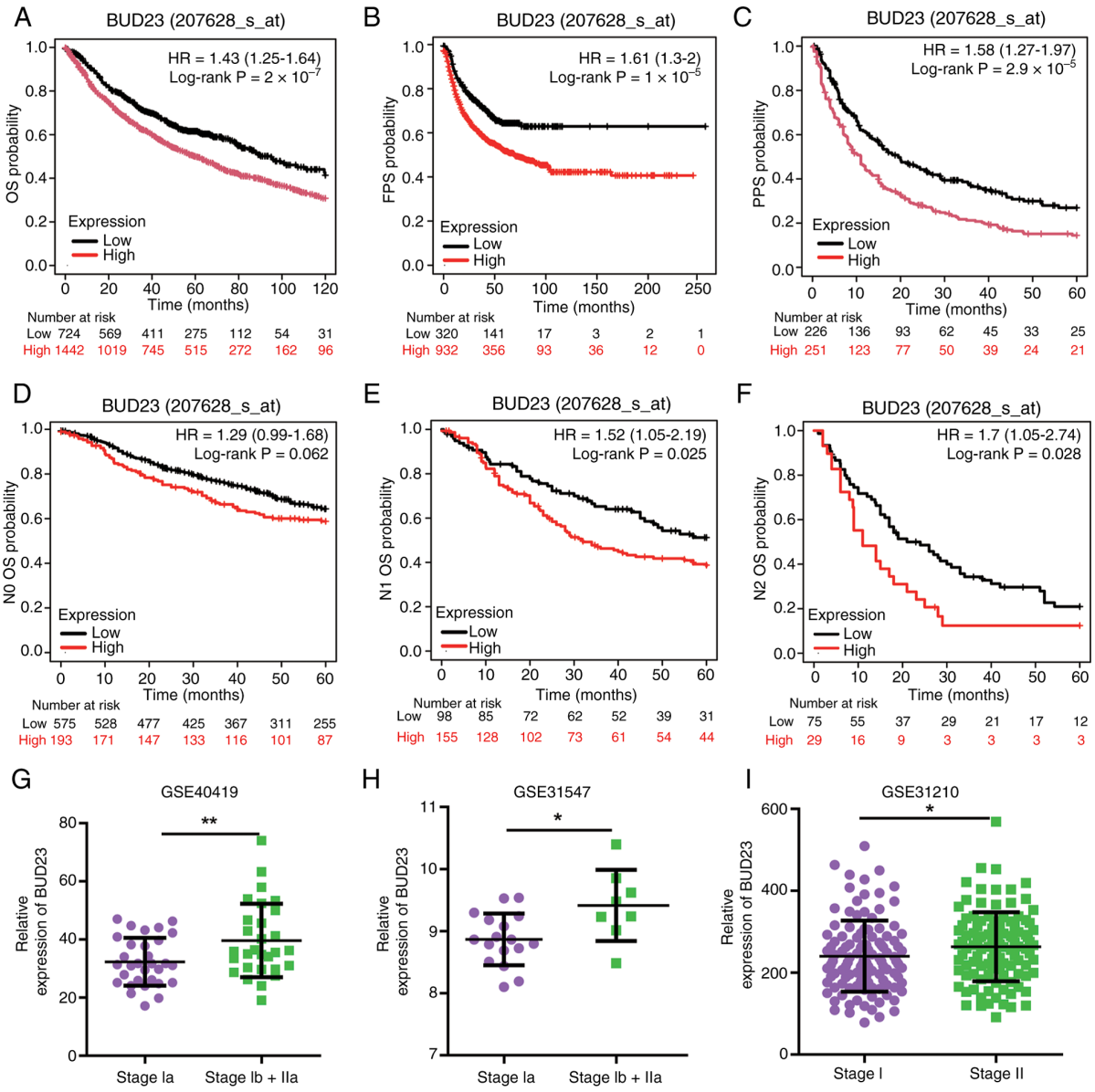

Figure 3. Elevated BUD23 levels are associated with poor clinical outcomes in patients with NSCLC. Kaplan-Meier survival curves comparing high and low BUD23 expression groups for (A) OS (n=2,166), (B) FPS (n=1252) and (C) PPS (n=447), generated using Kaplan-Meier Plotter. (D-F) Kaplan-Meier OS curves comparing high and low BUD23 expression groups in NSCLC stratified by N stage: (D) N0, (E) N1 and (F) N2. Association of BUD23 expression with different clinical stages of NSCLC based on analysis of the (G) GSE340419, (H) GSE31547 and (I) GSE31210 datasets. *P<0.05 and **P<0.01 as indicated. NSCLC, non-small cell lung cancer; OS, overall survival; FPS, first progression survival; PPS, post-progression survival; HR, hazard ratio (95% CI values).

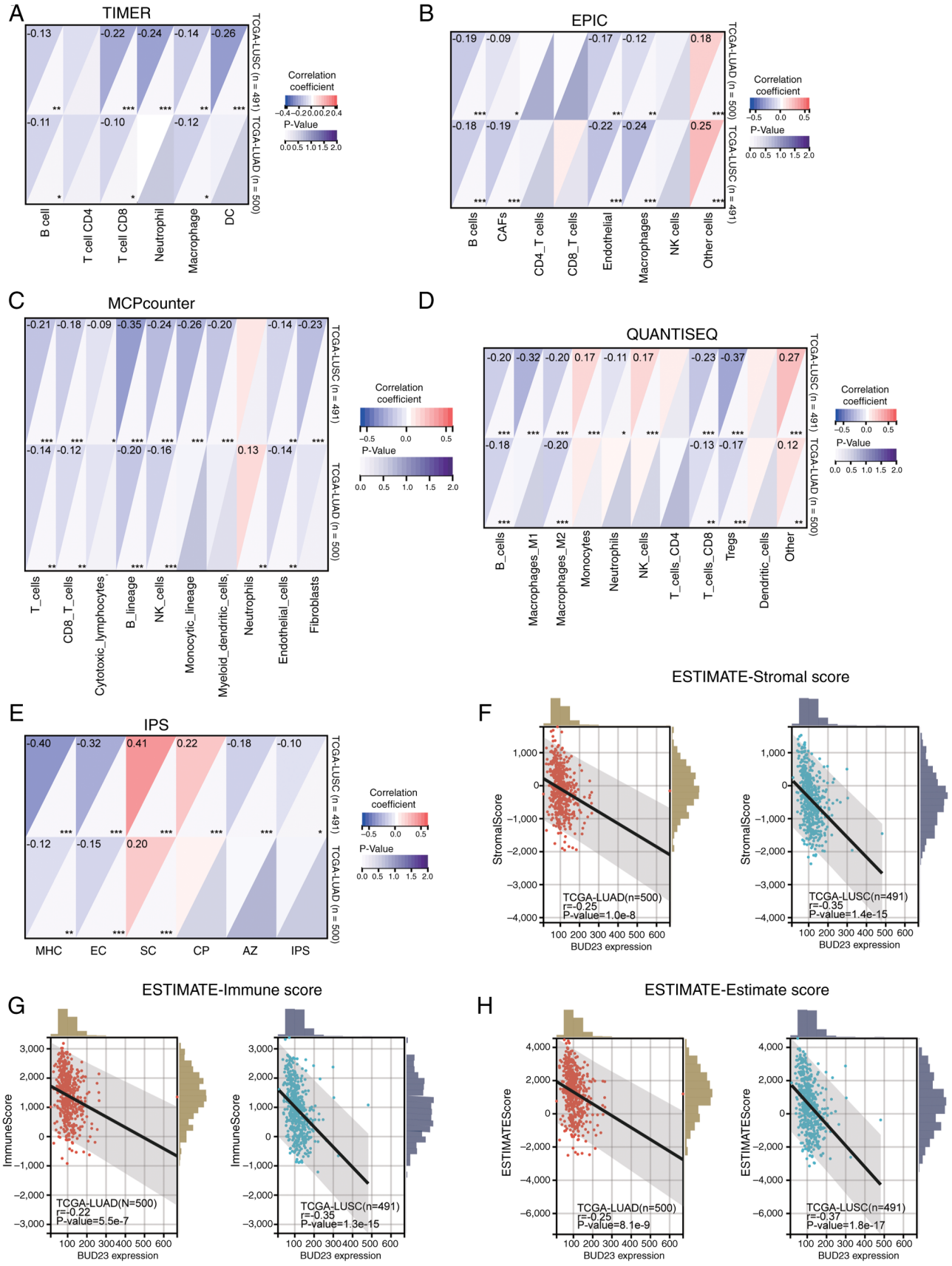

Figure 4. Correlation between BUD23 and immune characteristics in NSCLC analyzed using various algorithms based on TCGA-LUAD and -LUSC data. Correlations of BUD23 expression with the infiltration levels of (A) 6 immune cell types analyzed using TIMER, (B) 8 immune cell types analyzed using EPIC, (C) 10 immune cell types analyzed using MCPcounter and (D) 11 immune cell types of analyzed using QUANTISEQ. Correlations of BUD23 expression with (E) IPS score determined using the IPS algorithm and (F) stromal, (G) immune and (H) ESTIMATE scores analyzed using ESTIMATE. *P<0.05, **P<0.01 and ***P<0.001. NSCLC, non-small cell lung cancer; TCGA, The Cancer Genome Atlas; LUAD, lung adenocarcinoma; LUSC, lung squamous cell carcinoma; IPS, immunophenoscore; DC, dendritic cell; CAFs, cancer-associated fibroblasts; NK, natural killer; Tregs, regulatory T cells; MHC, major histocompatibility complex; EC, effector cell; SC, suppressor cell; CP, checkpoint molecule; AZ, antigen processing and presentation machinery.

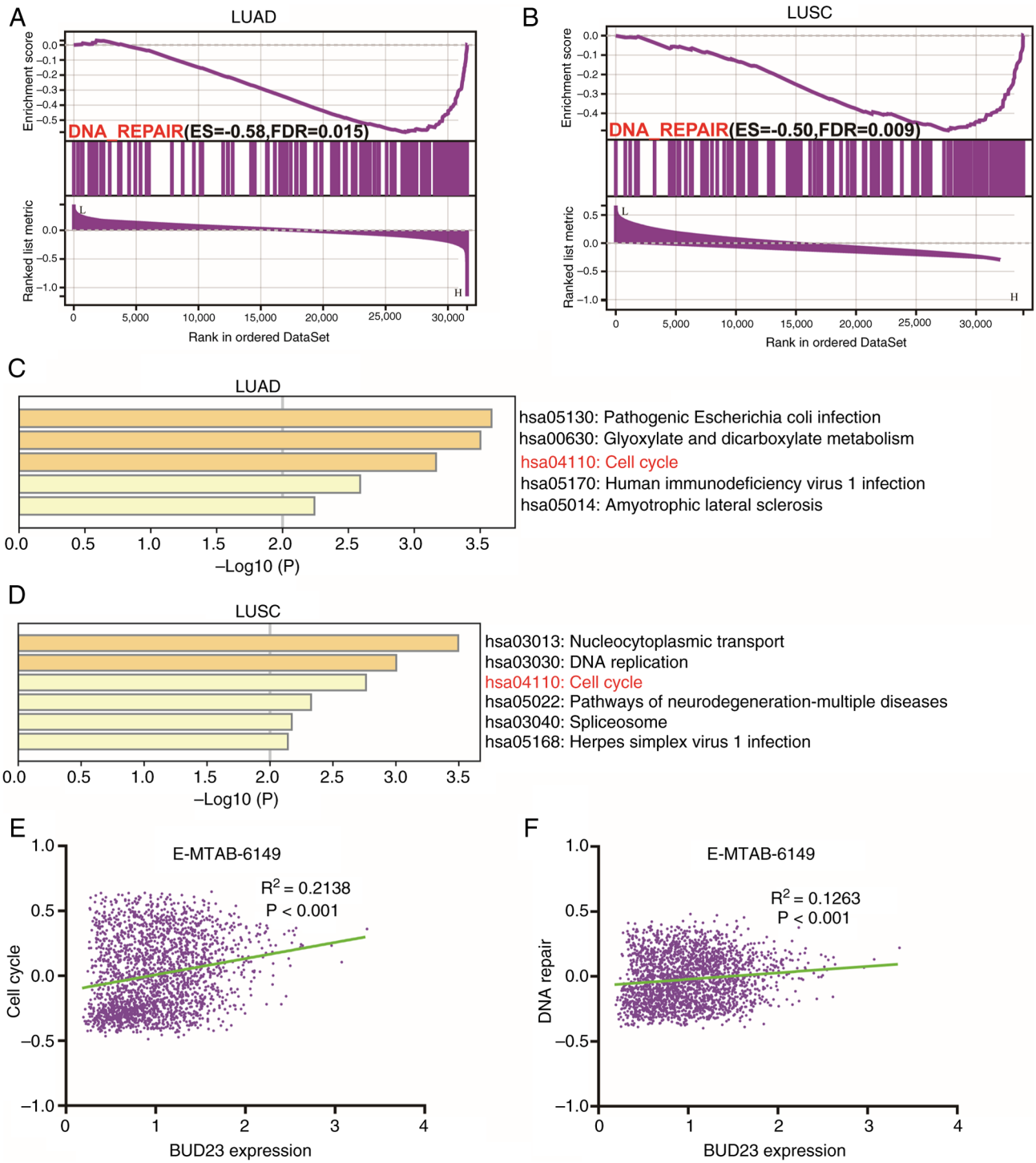

Figure 5. BUD23 is associated with DNA repair and cell cycle pathways in NSCLC. Gene set enrichment analysis analysis revealed that the Hallmark DNA repair gene set was significantly enriched in patients with high BUD23 expression in (A) TCGA-LUAD and (B) TCGA-LUSC cohorts. Kyoto Encyclopedia of Genes and Genomes pathway analysis revealed that BUD23-correlated genes (R^2>0.3, P<0.05) were significantly enriched in 'cell cycle' pathway in (C) TCGA-LUAD and (D) TCGA-LUSC. Single-cell correlation analysis based on the E-MTAB-6149 dataset in the CancerSEA database shows significant correlations between BUD23 expression and the (E) 'cell cycle' and (F) 'DNA repair' functional states in NSCLC. NSCLC, non-small cell lung cancer; TCGA, The Cancer Genome Atlas; LUAD, lung adenocarcinoma; LUSC, lung squamous cell carcinoma; ES, enrichment score; FDR, false discovery rate; -log10(P), -log10(P-value).

BUD23 knockdown suppresses the proliferative and migratory potential of NSCLC cells. To further elucidate the oncogenic role of BUD23 in NSCLC, its transcript levels in non-malignant human HBE cells and a panel of three NSCLC cell lines were compared. RT-qPCR revealed a significant upregulation of BUD23 expression in A549, H1299 and H460 cells compared with that in HBE cells (P<0.001; Fig. 6A). The siRNA-mediated depletion of BUD23 in A549 and H1299 cells significantly attenuated cell viability at the 48-h timepoint (P<0.001; Fig. 6B-E). Wound healing assays demonstrated that BUD23 knockdown also reduced the migratory capacity of A549 and H1299 cells after 48 h (P<0.01; Fig. 6F and G).

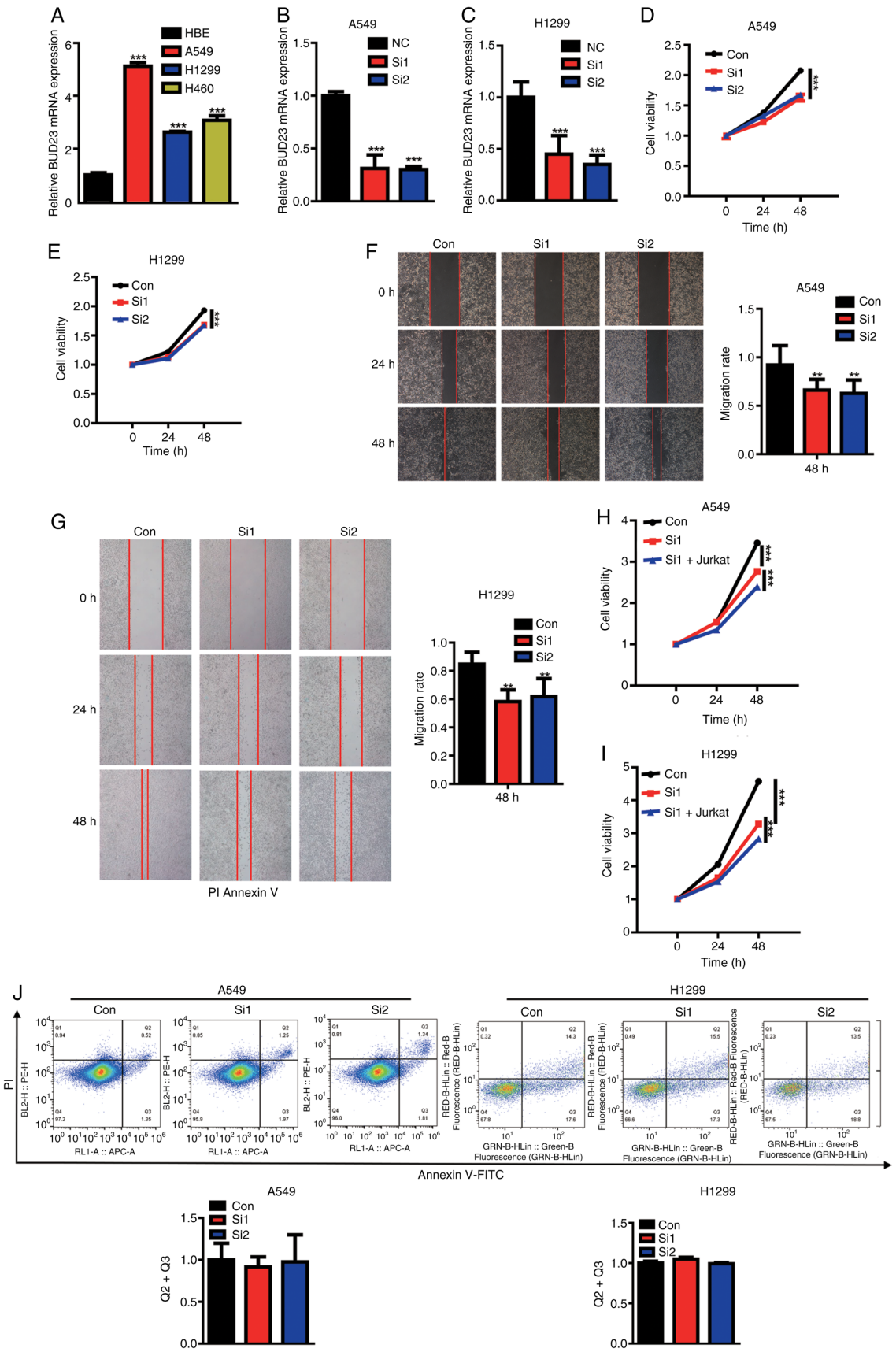

Figure 6. BUD23 knockdown suppresses the proliferative and migration of NSCLC cells. (A) RT-qPCR was used to quantify BUD23 mRNA levels in HBE cells and a panel of NSCLC cell lines. Validation of BUD23 knockdown efficiency in (B) A549 and (C) H1299 cells by RT-qPCR. Assessment of cell viability in (D) A549 and (E) H1299 cells via CCK-8 assay and cell migration in (F) A549 and (G) H1299 cells by wound healing assay (magnification, x10). CCK-8 assays of (H) A549 and (I) H1299 cells 24 h after BUD23 knockdown with or without subsequent co-culture with Jurkat T cells for 48 h in Transwell chambers. (J) Quantification of apoptosis in A549 and H1299 cells via Annexin V/PI flow cytometry. **P<0.01 and ***P<0.001 vs. HBE, NC, Con or as indicated. NSCLC, non-small cell lung cancer; RT-qPCR, reverse transcription-quantitative PCR; HBE, human bronchial epithelial; CCK-8, Cell Counting Kit-8; NC, negative control; Con, control; Si1/2, small interfering RNA targeting BUD23.

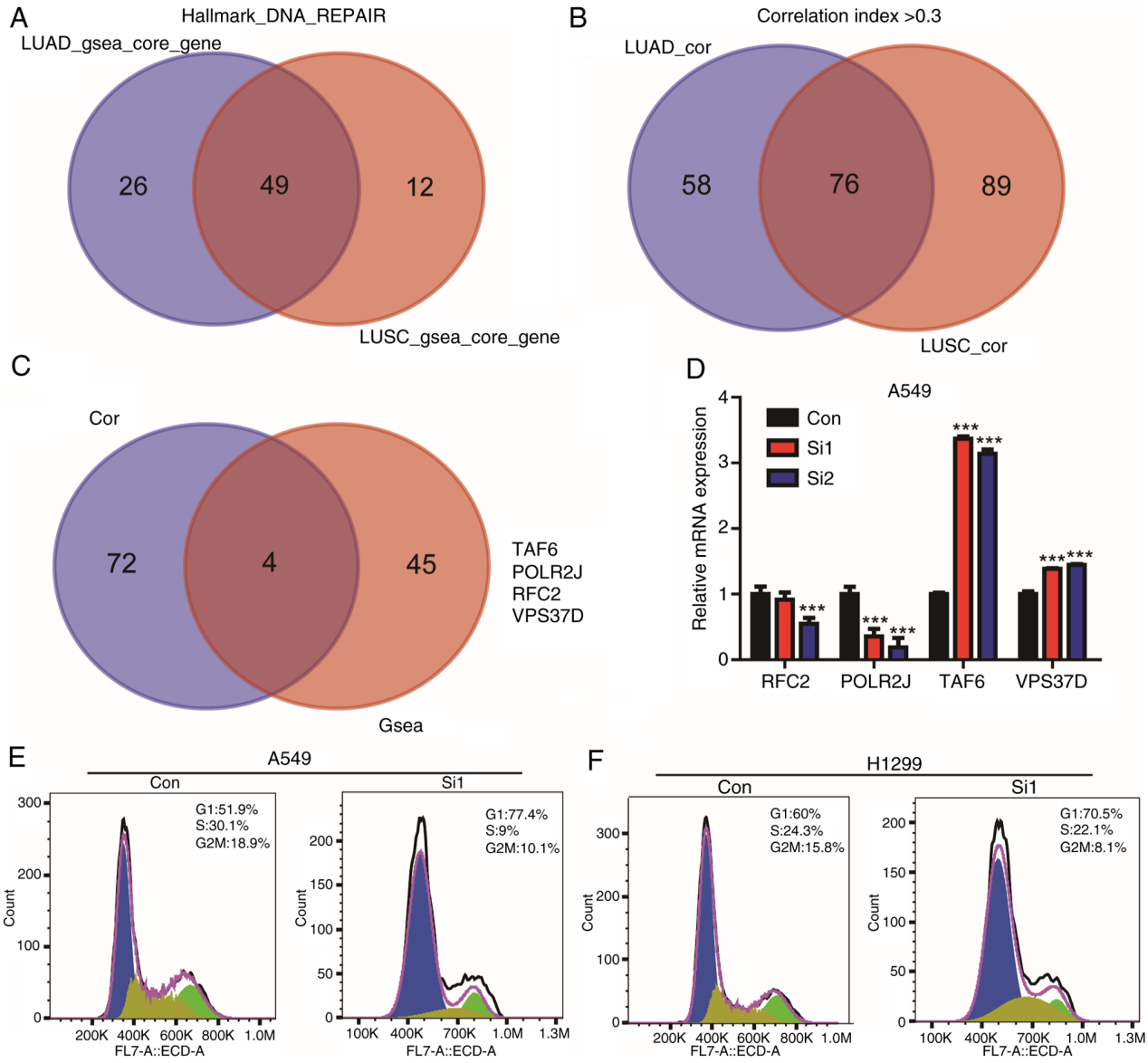

Figure 7. BUD23 knockdown significantly downregulates POLR2J expression in non-small cell lung cancer. (A) Venn diagram showing the intersection between LUAD GSEA core enrichment genes (key genes driving Hallmark DNA repair pathway enrichment) and LUSC GSEA core enrichment genes within the Hallmark DNA repair gene set, identifying 49 common genes. (B) Venn diagram showing the intersection between BUD23-correlated genes (correlation index >0.3) derived from the TCGA-LUAD cohort and BUD23-correlated genes (correlation index >0.3) derived from the TCGA-LUSC cohort via multi-gene correlation analysis, yielding 79 overlapping genes. (C) Venn diagram showing the secondary intersection between the 49 overlapping GSEA core enrichment genes (from panel A) and the 79 overlapping BUD23-correlated genes (from panel B), identifying 4 shared common genes: TAF6, POLR2J, RFC2 and VPS37D. (D) Validation of TAF6, POLR2J, RFC2 and VPS37D mRNA expression following BUD23 knockdown in A549 cells via reverse transcription-quantitative PCR. Cell-cycle analysis in (E) A549 and (F) H1299 cells following BUD23 knockdown. ***P<0.001 vs. Con. POLR2J, RNA polymerase II subunit J; LUAD, lung adenocarcinoma; GSEA, gene set enrichment analysis; LUSC, lung squamous cell carcinoma; TCGA, The Cancer Genome Atlas; TAF6, TATA-box binding protein associated factor 6; RFC2, replication factor C subunit 2; VPS37D, vacuolar protein sorting-associated protein 37D; Con, control; Si1, small interfering RNA targeting BUD23.

To investigate the relationship between BUD23 and immune infiltration, Jurkat T cells were co-cultured with A549 or H1299 cells and CCK-8 viability assays were subsequently performed. The results indicate that Jurkat T cells significantly increased the inhibitory effect of BUD23 knockdown on A549 and H1299 cell viability (P<0.001; Fig. 6H and I). By contrast, Annexin V/PI flow cytometry detected no significant difference in the apoptosis rates of A549 and H1299 following BUD23 knockdown (Fig. 6J). Collectively, these findings indicate that BUD23 silencing suppresses NSCLC cell proliferation and migration without inducing apoptosis.

BUD23 knockdown significantly downregulates POLR2J expression in NSCLC. To identify the critical downstream targets of BUD23, a hierarchical intersection strategy was used. GSEA revealed that BUD23 significantly modulates genes within the Hallmark DNA repair gene set (Fig. 5A and B). Intersection of the core-enriched genes from the GSEA of the TCGA-LUAD and -LUSC cohorts produced 49 candidates (Fig. 7A). The independent overlap of BUD23-correlated genes from the same two cohorts yielded 76 genes (Fig. 7B). Finally, the intersection of the 49 genes derived from the focused GSEA set with the 79 BUD23-correlated genes yielded four

high-confidence targets: TATA-box binding protein associated factor 6 (TAF6), RNA polymerase II subunit J (POLR2J), replication factor C subunit 2 (RFC2) and vacuolar protein sorting-associated protein 37D (VPS37D) (Fig. 7C). RT-qPCR validation confirmed that POLR2J expression is significantly attenuated following BUD23 knockdown in A549 cells and that only POLR2J expression exhibited the expected change (Fig. 7D). As DNA-repair processes are tightly associated with cell-cycle progression, the impact of BUD23 knockdown on the cell cycle of NSCLC cells was examined. The results revealed that BUD23 knockdown decreased the S- and G2-phase fractions in both A549 and H1299 cells (Fig. 7E and F). Collectively, these data suggest that POLR2J may be a BUD23-regulated effector involved in DNA repair in NSCLC.

Discussion

Lung cancer is the leading cause of cancer-related mortality worldwide. Therefore, elucidation of the molecular mechanisms underlying the development and progression of NSCLC is important to improve the prognosis of patients with this disease. In the present study, multi-omics profiling revealed pronounced BUD23 upregulation in NSCLC, which strongly predicts inferior patient outcomes. Integrative immunogenomic analysis further indicated that high BUD23 expression levels are associated with altered tumor immune infiltration. Mechanistically, GSEA, KEGG and single-cell pathway enrichment convergently implicated BUD23 in DNA-repair and cell-cycle networks that drive NSCLC progression. Functional experiments revealed that BUD23 depletion attenuated the proliferation and migration of NSCLC cells, and POLR2J was identified as a direct transcriptional target whose expression levels were markedly reduced following BUD23 knockdown. These findings provide a strong basis for future research into the role of BUD23 in the development and progression of NSCLC.

Previous studies have suggested that BUD23 is an oncogene, intimately associated with tumorigenesis and tumor progression, and with upregulated expression in various cancers, including breast cancer (12), myeloma (11), colorectal cancer (40) and hepatocellular carcinoma (41). Similarly, the differential analysis performed in the current study revealed upregulated BUD23 expression in NSCLC. Consistent findings were observed across multiple omics datasets through comparative analyses of tumor and normal tissues. Therefore, it can be concluded that BUD23 is upregulated in NSCLC. Further analysis revealed that elevated BUD23 expression is significantly associated with shorter OS, FPS and PPS, and an advanced clinical stage. These findings indicate that in NSCLC, patients with elevated BUD23 levels are likely to have worse clinical outcomes. Subgroup analysis revealed no statistically significant association between BUD23 expression and OS in patients with stage N0 NSCLC, although a trend towards shorter OS was observed in patients with high BUD23 expression. By contrast, patients with stage N1 or N2 NSCLC and high BUD23 expression exhibited a significantly shorter OS than those with these stages and low BUD23 expression. This may be attributed to BUD23 having a stronger association with advanced disease or the presence of additional confounding factors in patients with stage N0 NSCLC that could have influenced the results. These findings are consistent with a previous study, which found that high BUD23 expression predicted a shorter OS in patients with colorectal cancer (40). Similarly, a study of glioblastoma demonstrated that elevated BUD23 expression is associated with a poorer prognosis (10).

Multiple algorithms, including TIMER, EPIC, MCPcounter and QUANTISEQ, were employed in the present study to investigate the relationship between BUD23 and immune infiltration in NSCLC. The analysis consistently revealed a correlation between BUD23 and immune cell infiltration in NSCLC. Specifically, multiple algorithms indicated a negative correlation between BUD23 and the infiltration of B cells and $CD8^+$ T cells. Previous studies have shown that tumor-infiltrating B cells (TIL-Bs) play an important role in tumor immunology; specifically, TIL-Bs promote antitumor immunity by a unique antigen presentation pathway, which enhances T-cell activation, and TIL-B infiltration is positively associated with prognosis in multiple types of cancer (42,43). In the present study, high BUD23 expression was negatively correlated with B-cell infiltration, and associated with a poorer prognosis in patients with NSCLC. This suggests that BUD23 might influence patient prognosis by modulating B-cell immune infiltration. The *in vitro* experiments showed that in NSCLC cells, the knockdown of BUD23 enhanced the cytotoxic activity of Jurkat T cells. These *in vitro* data imply a potential association between BUD23 and tumor immune-related crosstalk. Similarly, previous research has established that $CD8^+$ T cells selectively kill tumor cells and play a crucial role in tumor immunotherapy (44). The negative correlation observed between BUD23 expression and $CD8^+$ T-cell infiltration suggest that patients with high BUD23 expression may exhibit diminished antitumor immune activity. The ESTIMATE algorithm is a method for calculating tumor purity. The present study revealed that BUD23 shows a negative correlation with stromal and immune scores in NSCLC, hinting that high BUD23 expression may be related to elevated tumor purity and decreased non-tumor cell infiltration, which could be implicated in the malignant progression of NSCLC. Collectively, these results imply a potential association between BUD23 expression and immune infiltration status within the NSCLC tumor microenvironment, which may partly account for the unfavorable prognosis in patients with NSCLC with high BUD23 expression.

The potential regulatory mechanisms by which BUD23 modulates the malignant progression of NSCLC were explored in the present study using various enrichment analyses. The results suggest that BUD23 might contribute to NSCLC progression by regulating DNA repair and cell cycle pathways, the latter being central to cell proliferation. A previous study has demonstrated that BUD23 promotes glioblastoma cell proliferation through the increased phosphorylation of AKT and increased expression of cyclin D1 and β-catenin (10). Notably, another study observed no significant change in BUD23 expression levels in HeLa cells subjected to UV irradiation (45). In the present study, *in vitro* data demonstrate that BUD23 contributes to the proliferative and migratory capacities of NSCLC cells. Knockdown of BUD23 affected the cell

cycle of NSCLC cells but not their apoptosis, suggesting that BUD23 does not affect apoptosis signaling and mainly affects pathways associated with cell viability and migration. While the precise underlying molecular mechanisms remain to be clarified, the present enrichment analysis, cell cycle assays and preliminary downstream gene expression data collectively provide partial clues supporting that BUD23 may regulate cell cycle progression via the activation of cell cycle checkpoints and alterations in cell cycle regulatory proteins. Other potential mechanisms, including metabolic reprogramming and intercellular crosstalk, represent purely speculative hypotheses without direct experimental support from the current study and warrant further in-depth investigation.

POLR2J emerged as a potential downstream target of BUD23 based on intersection analysis and RT-qPCR validation. Previous studies have implicated POLR2J as an oncogenic factor in multiple malignancies, including glioma (46), NSCLC (47), breast cancer (48), reproductive-system tumors (49) and colorectal carcinoma (50), where its upregulation has been associated with aggressive tumor behavior and adverse clinical outcomes. Therefore, these findings suggest that the BUD23-mediated control of POLR2J may be a previously unrecognized signaling axis influencing NSCLC progression. Nevertheless, further in-depth mechanistic analyses are urgently required to fully verify and characterize this novel regulatory axis.

However, several limitations of the present study should be acknowledged. First, although publicly available datasets and online analytic platforms enabled efficient data processing, they may introduce potential biases stemming from heterogeneous data collection protocols and patient baseline characteristics, while limiting in-depth mechanistic exploration. However, consistent results were obtained from multiple online databases and diverse data processing methods, which supports the reliability of the conclusions. Second, although analyses using multiple datasets and methods demonstrated an association of BUD23 expression with OS and immune infiltration in patients with NSCLC, BUD23 was not evaluated as a definitive prognostic predictor. Third, the mechanistic role of BUD23 in modulating immune infiltration, and its potential relevance to the response to checkpoint inhibitor therapy remains to be elucidated. However, it is planned to perform an immunohistochemical analysis of BUD23 expression and relevant immune markers in clinical lung cancer specimens to examine their correlations. Additionally, human NSCLC xenograft models coupled with immunohistochemical staining will be used to explore the relationship between BUD23 expression and solid tumor infiltration. Extensive *in vitro* and *in vivo* experiments, as well as additional clinical data, are necessary to validate the findings of the present study.

In summary, the collective findings of integrative multi-omics analyses in the present study reveal that BUD23 expression is markedly upregulated in NSCLC and its high expression portends a poor prognosis. Immunogenomic analyses revealed that elevated BUD23 expression is associated with alterations in immune cell infiltration levels. Functional enrichment analyses, including GSEA, KEGG and single-cell approaches, consistently implicate 'DNA repair' and 'cell cycle' pathways as processes associated with BUD23 expression. *In vitro* experiments demonstrated that siRNA-mediated BUD23 knockdown significantly attenuates NSCLC cell proliferation and migration, and POLR2J is a downstream target, the expression of which is markedly downregulated upon BUD23 depletion. These data provide convergent evidence that the present study indicates that the BUD23-POLR2J axis could act as a relevant regulatory module in NSCLC progression, highlighting BUD23 as a candidate prognostic biomarker and a promising therapeutic target for further investigation.

Acknowledgements

Not applicable.

Funding

No funding was received.

Availability of data and materials

The data generated in the present study may be requested from the corresponding author.

Authors' contributions

YT, JM and JZ performed the data analysis, experiments and figure preparation. JL conceived the study and participated in its design. JM and YT wrote the manuscript. YT and JL confirm the authenticity of all the raw data. All authors read and approved the final version of the manuscript.

Ethics approval and consent to participate

Not applicable.

Patient consent for publication

Not applicable.

Competing interests

The authors declare that they have no competing interests.

References

1. Bray F, Laversanne M, Sung H, Ferlay J, Siegel RL, Soerjomataram I and Jemal A: Global cancer statistics 2022: GLOBOCAN estimates of incidence and mortality worldwide for 36 cancers in 185 countries. CA Cancer J Clin 74: 229-263, 2024.
2. Marx A, Chan JK, Coindre JM, Detterbeck F, Girard N, Harris NL, Jaffe ES, Kurrer MO, Marom EM, Moreira AL, *et al*: The 2015 World Health Organization classification of tumors of the thymus: Continuity and changes. J Thorac Oncol 10: 1383-1395, 2015.
3. Adams SJ, Stone E, Baldwin DR, Vliegenthart R, Lee P and Fintelmann FJ: Lung cancer screening. Lancet 401: 390-408, 2023.
4. Asamura H, Nishimura KK, Giroux DJ, Chansky K, Hoering A, Rusch V and Rami-Porta R; Members of the IASLC Staging and Prognostic Factors Committee and of the Advisory Boards, and Participating Institutions: IASLC lung cancer staging project: The new database to inform revisions in the ninth edition of the TNM classification of lung cancer. J Thorac Oncol 18: 564-575, 2023.
5. Thai AA, Solomon BJ, Sequist LV, Gainor JF and Heist RS: Lung cancer. Lancet 398: 535-554, 2021.

6. Ferrari M and Stagi S: Oxidative stress in down and williams-beuren syndromes: An overview. Molecules 26: 3139, 2021.
7. Zorbas C, Nicolas E, Wacheul L, Huvelle E, Heurgué-Hamard V and Lafontaine DL: The human 18S rRNA base methyltransferases DIMT1L and WBSCR22-TRMT112 but not rRNA modification are required for ribosome biogenesis. Mol Biol Cell 26: 2080-2095, 2015.
8. Petrossian TC and Clarke SG: Uncovering the human methyltransferasome. Mol Cell Proteomics 10: M110.000976, 2011.
9. Õunap K, Käsper L, Kurg A and Kurg R: The human WBSCR22 protein is involved in the biogenesis of the 40S ribosomal subunits in mammalian cells. PLoS One 8: e75686, 2013.
10. Chi Y, Liang Z, Guo Y, Chen D, Lu L, Lin J, Qiu S, Wang X, Qiu E, Lin F, *et al*: WBSCR22 confers cell survival and predicts poor prognosis in glioma. Brain Res Bull 161: 1-12, 2020.
11. Tiedemann RE, Zhu YX, Schmidt J, Shi CX, Sereduk C, Yin H, Mousses S and Stewart AK: Identification of molecular vulnerabilities in human multiple myeloma cells by RNA interference lethality screening of the druggable genome. Cancer Res 72: 757-768, 2012.
12. Nakazawa Y, Arai H and Fujita N: The novel metastasis promoter Merm1/Wbscr22 enhances tumor cell survival in the vasculature by suppressing Zac1/p53-dependent apoptosis. Cancer Res 71: 1146-1155, 2011.
13. Khan AA, Huang H, Zhao Y, Li H, Pan R, Wang S and Liu X: WBSCR22 and TRMT112 synergistically suppress cell proliferation, invasion and tumorigenesis in pancreatic cancer via transcriptional regulation of ISG15. Int J Oncol 60: 24, 2022.
14. Yan D, Zheng X, Tu L, Jia J, Li Q, Cheng L and Wang X: Knockdown of Merm1/Wbscr22 attenuates sensitivity of H460 non-small cell lung cancer cells to SN-38 and 5-FU without alteration to p53 expression levels. Mol Med Rep 11: 295-302, 2015.
15. Gillette MA, Satpathy S, Cao S, Dhanasekaran S, Vasaikar S, Krug K, Petralia F, Li Y, Liang WW, Reva B, *et al*: A02 Proteogenomic characterization reveals therapeutic vulnerabilities in lung adenocarcinoma. J Thorac Oncol 15 (Suppl): S12, 2020.
16. Satpathy S, Krug K, Jean Beltran PM, Savage SR, Petralia F, Kumar-Sinha C, Dou Y, Reva B, Kane MH, Avanessian SC, *et al*: A proteogenomic portrait of lung squamous cell carcinoma. Cell 184: 4348-4371.e40, 2021.
17. Rousseaux S, Debernardi A, Jacquiau B, Vitte AL, Vesin A, Nagy-Mignotte H, Moro-Sibilot D, Brichon PY, Lantuejoul S, Hainaut P, *et al*: Ectopic activation of germline and placental genes identifies aggressive metastasis-prone lung cancers. Sci Transl Med 5: 186ra66, 2013.
18. Hou J, Aerts J, den Hamer B, van Ijcken W, den Bakker M, Riegman P, van der Leest C, van der Spek P, Foekens JA, Hoogsteden HC, *et al*: Gene expression-based classification of non-small cell lung carcinomas and survival prediction. PLoS One 5: e10312, 2010.
19. Zhang Y, Foreman O, Wigle DA, Kosari F, Vasmatzis G, Salisbury JL, van Deursen J and Galardy PJ: USP44 regulates centrosome positioning to prevent aneuploidy and suppress tumorigenesis. J Clin Invest 122: 4362-4374, 2012.
20. Kim IJ, Quigley D, To MD, Pham P, Lin K, Jo B, Jen KY, Raz D, Kim J, Mao JH, *et al*: Rewiring of human lung cell lineage and mitotic networks in lung adenocarcinomas. Nat Commun 4: 1701, 2013.
21. Seo JS, Ju YS, Lee WC, Shin JY, Lee JK, Bleazard T, Lee J, Jung YJ, Kim JO, Shin JY, *et al*: The transcriptional landscape and mutational profile of lung adenocarcinoma. Genome Res 22: 2109-2119, 2012.
22. Girard L, Rodriguez-Canales J, Behrens C, Thompson DM, Botros IW, Tang H, Xie Y, Rekhtman N, Travis WD, Wistuba II, *et al*: An expression signature as an aid to the histologic classification of non-small cell lung cancer. Clin Cancer Res 22: 4880-4889, 2016.
23. Chen CH, Lai JM, Chou TY, Chen CY, Su LJ, Lee YC, Cheng TS, Hong YR, Chou CK, Whang-Peng J, *et al*: VEGFA upregulates FLJ10540 and modulates migration and invasion of lung cancer via PI3K/AKT pathway. PLoS One 4: e5052, 2009.
24. Wei TY, Juan CC, Hisa JY, Su LJ, Lee YC, Chou HY, Chen JM, Wu YC, Chiu SC, Hsu CP, *et al*: Protein arginine methyltransferase 5 is a potential oncoprotein that upregulates G1 cyclins/cyclin-dependent kinases and the phosphoinositide 3-kinase/AKT signaling cascade. Cancer Sci 103: 1640-1650, 2012.
25. Robles AI, Arai E, Mathé EA, Okayama H, Schetter AJ, Brown D, Petersen D, Bowman ED, Noro R, Welsh JA, *et al*: An integrated prognostic classifier for stage I lung adenocarcinoma based on mRNA, microRNA, and DNA methylation biomarkers. J Thorac Oncol 10: 1037-1048, 2015.
26. Sun Z, Wang L, Eckloff BW, Deng B, Wang Y, Wampfler JA, Jang J, Wieben ED, Jen J, You M and Yang P: Conserved recurrent gene mutations correlate with pathway deregulation and clinical outcomes of lung adenocarcinoma in never-smokers. BMC Med Genomics 7: 32, 2014.
27. Li J, Wang B, Li X and Zhu Y: Estimation of hub genes and infiltrating immune cells in non-smoking females with lung adenocarcinoma by integrated bioinformatic analysis. Med Sci Monitor 26: e922680, 2020.
28. Okayama H, Kohno T, Ishii Y, Shimada Y, Shiraishi K, Iwakawa R, Furuta K, Tsuta K, Shibata T, Yamamoto S, *et al*: Identification of genes upregulated in ALK-positive and EGFR/KRAS/ALK-negative lung adenocarcinomas. Cancer Res 72: 100-111, 2012.
29. Győrffy B, Surowiak P, Budczies J and Lánczky A: Online survival analysis software to assess the prognostic value of biomarkers using transcriptomic data in non-small-cell lung cancer. PLoS One 8: e82241, 2013.
30. Li T, Fan J, Wang B, Traugh N, Chen Q, Liu JS, Li B and Liu XS: TIMER: A web server for comprehensive analysis of tumor-infiltrating immune cells. Cancer Res 77: e108-e110, 2017.
31. Racle J, de Jonge K, Baumgaertner P, Speiser DE and Gfeller D: Simultaneous enumeration of cancer and immune cell types from bulk tumor gene expression data. Elife 6: e26476, 2017.
32. Becht E, Giraldo NA, Lacroix L, Buttard B, Elarouci N, Petitprez F, Selves J, Laurent-Puig P, Sautès-Fridman C, Fridman WH and de Reyniès A: Estimating the population abundance of tissue-infiltrating immune and stromal cell populations using gene expression. Genome Biol 17: 218, 2016.
33. Finotello F, Mayer C, Plattner C, Laschober G, Rieder D, Hackl H, Krogsdam A, Loncova Z, Posch W, Wilflingseder D, *et al*: Molecular and pharmacological modulators of the tumor immune contexture revealed by deconvolution of RNA-seq data. Genome Med 11: 34, 2019.
34. Yoshihara K, Shahmoradgoli M, Martínez E, Vegesna R, Kim H, Torres-Garcia W, Treviño V, Shen H, Laird PW, Levine DA, *et al*: Inferring tumour purity and stromal and immune cell admixture from expression data. Nat Commun 4: 2612, 2013.
35. Charoentong P, Finotello F, Angelova M, Mayer C, Efremova M, Rieder D, Hackl H and Trajanoski Z: Pan-cancer immunogenomic analyses reveal genotype-immunophenotype relationships and predictors of response to checkpoint blockade. Cell Rep 18: 248-262, 2017.
36. Chandrashekar DS, Karthikeyan SK, Korla PK, Patel H, Shovon AR, Athar M, Netto GJ, Qin ZS, Kumar S, Manne U, *et al*: UALCAN: An update to the integrated cancer data analysis platform. Neoplasia 25: 18-27, 2022.
37. Yuan H, Yan M, Zhang G, Liu W, Deng C, Liao G, Xu L, Luo T, Yan H, Long Z, *et al*: CancerSEA: A cancer single-cell state atlas. Nucl Acids Res 47 (D1): D900-D908, 2019.
38. Livak KJ and Schmittgen TD: Analysis of relative gene expression data using real-time quantitative PCR and the 2(-Delta Delta C(T)) method. Methods 25: 402-408, 2001.
39. Aliazis K, Christofides A, Shah R, Yeo YY, Jiang S, Charest A and Boussiotis VA: The tumor microenvironment's role in the response to immune checkpoint blockade. Nat Cancer 6: 924-937, 2025.
40. Yan D, Tu L, Yuan H, Fang J, Cheng L, Zheng X and Wang X: WBSCR22 confers oxaliplatin resistance in human colorectal cancer. Sci Rep 7: 15443, 2017.
41. Stefanska B, Cheishvili D, Suderman M, Arakelian A, Huang J, Hallett M, Han ZG, Al-Mahtab M, Akbar SM, Khan WA, *et al*: Genome-wide study of hypomethylated and induced genes in patients with liver cancer unravels novel anticancer targets. Clin Cancer Res 20: 3118-3132, 2014.
42. Petitprez F, de Reyniès A, Keung EZ, Chen TW, Sun CM, Calderaro J, Jeng YM, Hsiao LP, Lacroix L, Bougoüin A, *et al*: B cells are associated with survival and immunotherapy response in sarcoma. Nature 577: 556-560, 2020.
43. Helmink BA, Reddy SM, Gao J, Zhang S, Basar R, Thakur R, Yizhak K, Sade-Feldman M, Blando J, Han G, *et al*: B cells and tertiary lymphoid structures promote immunotherapy response. Nature 577: 549-555, 2020.

44. Philip M, Fairchild L, Sun L, Viale A, Merghoub T, Wolchok JD, Leslie CS and Schietinger A: Chromatin state dynamics underlying CD8 T cell differentiation and dysfunction in cancer. Blood 128: 861, 2016.
45. Stixová L, Tichý V and Bártová E: RNA-related DNA damage and repair: The role of N7-methylguanosine in the cell nucleus exposed to UV light. Heliyon 10: e25599, 2024.
46. Zheng XL, Li ZD, Luo KZ, Li YL, Liu YH, Shen SY, Shen FY, Li WY, Chen GQ, Zhang C and Zeng LH: POLR2J expression promotes glioblastoma malignancy by regulating oxidative stress and the STAT3 signaling pathway. Am J Cancer Res 14: 2037-2054, 2024.
47. Campbell JM, Lockwood WW, Buys TP, Chari R, Coe BP, Lam S and Lam WL: Integrative genomic and gene expression analysis of chromosome 7 identified novel oncogene loci in non-small cell lung cancer. Genome 51: 1032-1039, 2008.
48. Nourbakhsh M, Saksager A, Tom N, Chen XS, Colaprico A, Olsen C, Tiberti M and Papaleo E: A workflow to study mechanistic indicators for driver gene prediction with moonlight. Brief Bioinform 24: bbad274, 2023.
49. Yao L, Cong R, Ji C, Zhou X, Luan J, Meng X and Song N: RNA-binding proteins play an important role in the prognosis of patients with testicular germ cell tumor. Front Genet 12: 610291, 2021.
50. Costales-Carrera A, Fernández-Barral A, Bustamante-Madrid P, Domínguez O, Guerra-Pastrián L, Cantero R, Del Peso L, Burgos A, Barbáchano A and Muñoz A: Comparative study of organoids from patient-derived normal and tumor colon and rectal tissue. Cancers (Basel) 12: 2302, 2020.